Evaluation of the Effects of Rotor Harmonics in a Doubly-Fed Induction Generator With Harmonic Induced Speed Ripple

Yong Liao, Li Ran, *Member, IEEE*, Ghanim A. Putrus, and Kenneth S. Smith, *Member, IEEE*

***Abstract*—This paper is concerned with the low-frequency harmonics which originate from the rotor inverter of a doubly-fed induction generator (DFIG). By including the mechanical speed response, it expands the transformer approach previously taken to analyze the harmonic transfer in the machine. A numerical method is proposed to calculate the stator current sidebands, which can be used to predict the voltage fluctuation at the system busbar. It is shown that the pulsating torque associated with the rotor harmonics can induce speed ripple depending on the inertia, causing a significant change in the stator current spectrum. Experiment and simulation verify the analysis and the proposed calculation method.**

***Index Terms*—Doubly-fed induction generator, harmonics, modulation, pulsating torque, spectrum.**

I. Introduction

A DOUBLY-FED induction generator (DFIG) is based on a wound rotor induction machine. The three-phase rotor windings are supplied with a voltage of controllable amplitude and frequency using a static power electronic converter. Consequently, the speed can be varied while the operating frequency on the stator side remains constant. Depending on the required speed range, the rotor converter rating is usually small compared to the machine rating. Therefore, a DFIG is ideal for applications such as wind, pumped storage, and micro-hydro power plants which inherently favor variable speed operation [1], [2]. It is also attractive to other dispersed generation schemes where the fuel efficiency can be improved if the diesel engine or gas turbine is allowed to run at variable speed according to the load level [3].

There is increasing concern about the rotor side harmonics in doubly-fed induction generators. The converter provides a fundamental voltage at the slip frequency, and for the reasons to be explained later, the associated low-frequency harmonics can cause a pulsating air-gap torque and voltage fluctuation on the system busbar. Since the impedance viewed from the rotor side of the machine is small at low slip frequency, such effects can be very detrimental in practice. With a direct ac-ac cycloconverter, low-frequency harmonics can be produced as a result of the modulation process between the input and output frequencies [4], [5]. It will be shown in this paper that such low-frequency harmonics can also exist in a PWM inverter having a high switching frequency. In wind power systems, pulsating torque and flicker have already occurred caused by a fluctuating input due to wind speed variation [6]. The effects caused by the rotor side harmonics as discussed in this study will further add to the scenario.

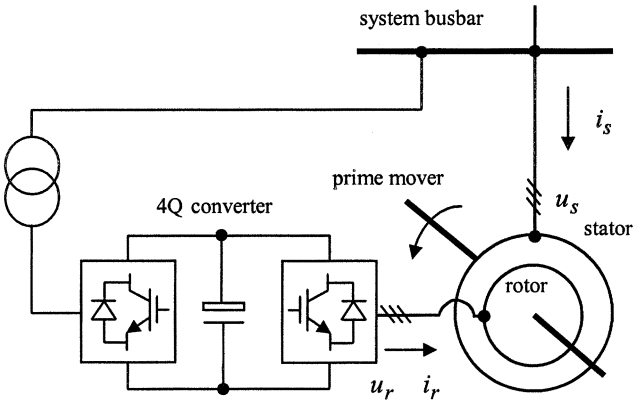

Fig. 1. System configuration.

Previous researchers have considered the transfer of harmonics from the rotor to the stator side of the machine, which was assumed to follow the transformer principle [i.e., magnetomotive force (mmf) balance] on both sides [7]–[9]. The standard equivalent circuit of an induction machine was modified to calculate the stator current and voltage harmonics, and frequency modulation was handled by considering the slip. It has been shown previously that the mechanical behavior will reflect electrically in a cage induction machine [10]. Using these results, this study will further the analysis by including the mechanical speed response in the model. Inclusion of the speed ripple will significantly improve the model accuracy. After a better understanding of the electromechanical interaction in the DFIG is obtained, it would be possible to improve the overall performance of the generator system by, for example, controlling the rotor side inverter.

II. Generator Model

The configuration of a DFIG system is shown in Fig. 1. In order to analyze the harmonics with electromechanical interac-

Manuscript received October 24, 2002. This work was supported in part by Northumbria University and in part by the Cheung Kong Scholar Program of China.

Y. Liao is with Chongqing University, Chongqing 400044, China (e-mail: yongliaocqu@cta.cq.cn).

L. Ran is with the School of Engineering, University of Durham, Durham DH1 3LE, U.K. (e-mail: li.ran@durham.ac.uk).

G. A. Putrus is with the Northumbria University, Newcastle upon Tyne NE1 8ST, U.K. (e-mail: ghanim.putrus@unn.ac.uk).

K. S. Smith is with the Mott MacDonald, Power Systems Division, Glasgow G2 8YD, U.K. (e-mail: KSS@sas-glas.mottmac.com).

Digital Object Identifier 10.1109/TEC.2003.816606

tions in the system, a model of the machine should be established to relate the rotor and stator voltages and currents as well as the air-gap torque and the rotor speed. In a steady-state, each variable consists of a series of Fourier components at different frequencies. The flux linkage equation is [11]

$$\begin{bmatrix}\psi_s\\ \psi_r\end{bmatrix}=\begin{bmatrix}L_s & M_{sr}\\ M_{rs} & L_r\end{bmatrix}\begin{bmatrix}i_s\\ i_r\end{bmatrix}. \tag{1}$$

Subscripts "s" and "r" stand for the stator and rotor windings, respectively; each side includes three phases, and amplitudes of the rotor side quantities are referred to the stator side. Note that quantities on both sides are expressed in their own frequencies. The inductance matrices are defined as follows where the mutual elements between the stator and rotor windings depend on the rotor electrical angle θ. M is the mutual inductance coefficient (i.e., 3/2 of the magnetizing inductance in the normal equivalent circuit). L_{ls} and L_{lr} are the leakage inductances of the stator and rotor windings.

$$L_s=\begin{bmatrix}L_{ls}+M & -\frac{M}{3} & -\frac{M}{3}\\ -\frac{M}{3} & L_{ls}+M & -\frac{M}{3}\\ -\frac{M}{3} & -\frac{M}{3} & L_{ls}+M\end{bmatrix} \tag{2}$$

$$L_r=\begin{bmatrix}L_{lr}+M & -\frac{M}{3} & -\frac{M}{3}\\ -\frac{M}{3} & L_{lr}+M & -\frac{M}{3}\\ -\frac{M}{3} & -\frac{M}{3} & L_{lr}+M\end{bmatrix} \tag{3}$$

$$M_{sr}=M_{rs}^T=\frac{2M}{3}\begin{bmatrix}\cos\theta & \cos\left(\theta+\frac{2\pi}{3}\right) & \cos\left(\theta-\frac{2\pi}{3}\right)\\ \cos\left(\theta-\frac{2\pi}{3}\right) & \cos\theta & \cos\left(\theta+\frac{2\pi}{3}\right)\\ \cos\left(\theta+\frac{2\pi}{3}\right) & \cos\left(\theta-\frac{2\pi}{3}\right) & \cos\theta\end{bmatrix} \tag{4}$$

In a steady-state condition without any speed ripple, $\theta=(1-s)\omega t$, where s is the slip and ω is the synchronous electrical frequency. The fundamental components of the stator and rotor currents are at frequencies ω and $s\omega$, respectively. It can be shown that the product of M_{sr} and i_r gives terms at the stator frequency while the product of M_{rs} and i_s will produce terms at the rotor or slip frequency. Denoting the winding voltages $u=[u_s^T\ u_r^T]^T$, currents $i=[i_s^T\ i_r^T]^T$, L as the total inductance matrix, and R as the resistance matrix, the voltage balance equation of the machine can be derived as

$$u=Ri+\frac{d}{dt}(Li)=(R+pL+Lp)i=Zi \tag{5}$$

where $Z=R+pL+Lp$ is the total "impedance matrix" of the machine, and p is the "d/dt" derivative operator. In deriving (5), it was noticed that the inductance matrix L depends on the rotor angle and, hence, is time-variant. Therefore, $d/dt(Li)=dL/dt\cdot i+L\cdot di/dt=pL\cdot i+L\cdot pi$. According to (5), harmonics in the rotor supply voltage will cause harmonic currents on both the stator and rotor sides of the machine. Due to the interactions between the mmfs established by the stator and rotor currents, harmonics exist in the machine torque which will lead to speed ripple. With the self-inductances of the windings being constant in a round rotor machine, the air-gap torque can be calculated as below based on the "coenergy" principle [11]

$$T_e=\frac{P}{2}\frac{1}{2}i^T\begin{bmatrix}0 & \frac{\partial M_{sr}}{\partial\theta}\\ \frac{\partial M_{rs}}{\partial\theta} & 0\end{bmatrix}i \tag{6}$$

where P is the number of poles of the machine. The speed ripple will then be reflected in the impedance matrix, further affecting the harmonic content of the current and torque.

III. Extra Harmonic Excitation Due to Speed Ripple

It is initially assumed that the speed signal contains only one ripple component. A general case can be considered using superposition. The electrical speed is given by

$$\omega_{rotor}=\omega_0+A_r\sin(\omega_r t+\alpha_0-\pi) \tag{7}$$

where ω_0 is the average speed, A_r the amplitude, and ω_r the frequency of the speed ripple. ω_0 and A_r are both in rad/s. The rotor electrical angle is calculated as follows including a linear term due to the average speed and a disturbance term corresponding to the speed ripple:

$$\theta=\omega_0 t+\frac{A_r}{\omega_r}\cos(\omega_r t+\alpha_0). \tag{8}$$

As the disturbance term is relatively small, the following approximations are justifiable:

$$\cos\left[\frac{A_r}{\omega_r}\cos(\omega_r t+\alpha_0)\right]\approx 1 \tag{9}$$

$$\sin\left[\frac{A_r}{\omega_r}\cos(\omega_r t+\alpha_0)\right]\approx\frac{A_r}{\omega_r}\cos(\omega_r t+\alpha_0). \tag{10}$$

Using these approximations, it can be shown that the immediate effect of the speed ripple is to cause the following increment to the impedance matrix which depends on the rotor angle:

$$\Delta Z=\Delta Z_1+\Delta Z_2+\Delta Z_3+\Delta Z_4 \tag{11}$$

where

$$\Delta Z_1=\frac{MA_r}{3\omega_r}(\omega_0+\omega_r)\begin{bmatrix}0 & C_{\omega_0+\omega_r}\\ C_{\omega_0+\omega_r}^T & 0\end{bmatrix} \tag{12}$$

$$\Delta Z_2=\frac{MA_r}{3\omega_r}(\omega_0-\omega_r)\begin{bmatrix}0 & C_{\omega_0-\omega_r}\\ C_{\omega_0-\omega_r}^T & 0\end{bmatrix} \tag{13}$$

$$\Delta Z_3=\frac{MA_r}{3\omega_r}\begin{bmatrix}0 & D_{\omega_0+\omega_r}\\ D_{\omega_0+\omega_r}^T & 0\end{bmatrix}p \tag{14}$$

$$\Delta Z_4=\frac{MA_r}{3\omega_r}\begin{bmatrix}0 & D_{\omega_0-\omega_r}\\ D_{\omega_0-\omega_r}^T & 0\end{bmatrix}p \tag{15}$$

where the elements in submatrices $C_{\omega_0+\omega_r}$, $C_{\omega_0-\omega_r}$, $D_{\omega_0+\omega_r}$, and $D_{\omega_0-\omega_r}$, are at frequency $\omega_0+\omega_r$ or $\omega_0-\omega_r$ as the subscript indicates. These elements are expanded in Appendix A which also outlines the derivation process. Due to the increment of the impedance matrix ΔZ, both the voltage and current vectors of the machine will have an increment, Δu and Δi, respectively. According to (5)

$$\begin{aligned}u+\Delta u&=(Z+\Delta Z)(i+\Delta i)\\ &=Zi+\Delta Zi+Z\Delta i+\Delta Z\Delta i.\end{aligned} \tag{16}$$

As $u=Zi$, the incremental voltage, current, and impedance are interrelated as follows:

$$\Delta u=\Delta Zi+Z\Delta i+\Delta Z\Delta i. \tag{17}$$

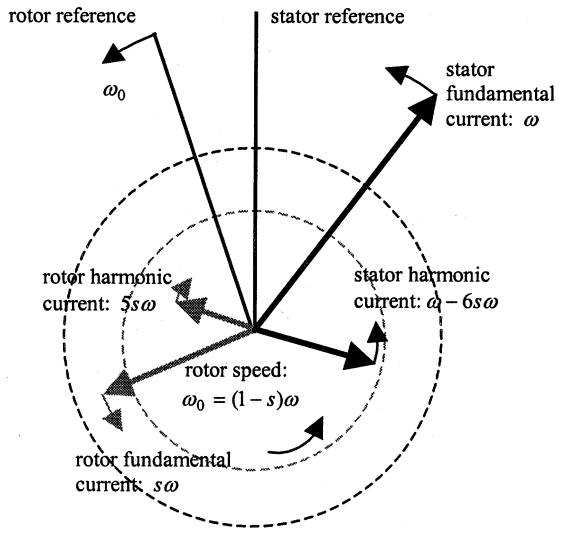

Fig. 2. Balance of mmf associated with stator and rotor currents.

TABLE I
HARMONIC FREQUENCIES WITH THE EFFECT OF SPEED RIPPLE

Reference of observation	Stator	Rotor
Modulation mechanism	ω , $\omega - \omega_r$, $\omega + \omega_r$, $\omega - 2\omega_r$, $\omega + 2\omega_r$, ...	$s\omega$, $s\omega - \omega_r$, $s\omega + \omega_r$, $s\omega - 2\omega_r$, $s\omega + 2\omega_r$, ...
Numerical example (Hz)	50 Hz, 44 Hz, 56 Hz, 38 Hz, 62 Hz,...	1 Hz, -5 Hz, 7 Hz, -11 Hz, 13 Hz, ...

Equation (17) shows the mechanism which determines the harmonics observed on the two sides of the DFIG [12]. To illustrate the mechanism, a comparison is made between cases with and without speed ripple. Suppose the rotor supply contains only a fifth harmonic current which is of negative phase sequence. Without speed ripple, the corresponding mmf rotates backward at six times of the slip frequency with respect to the stator fundamental. In order to balance the mmf, the stator current will contain a component of positive phase sequence and at frequency $\omega - 6s\omega$ [13]. This case of interaction is depicted in Fig. 2.

In this case, torque ripple will be caused at the sixth harmonic frequency of the rotor fundamental. As the rotor speed varies, the frequency of the current induced on the stator side must change. A series of new modulation terms at various frequencies will be produced. Increment of the impedance matrix is involved in this interactive process. According to (17), the rotor current at frequency $s\omega$ will modulate with terms in ΔZ at frequencies $\omega_0 \pm \omega_r$ to give excitation voltages on the stator side at frequencies $\omega_0 + s\omega \pm \omega_r$ (i.e., $\omega \pm \omega_r$). Stator current and voltage components as sidebands of the fundamental are caused. Thus, a component at frequency $\omega + 6s\omega$ is also present in addition to the one at frequency $\omega - 6s\omega$. Similarly, the fundamental stator current will also modulate with ΔZ to excite harmonics on the rotor side. The other two terms in (17) will cause extra components. Table I shows the generation of the sideband frequencies due to the speed ripple. It is assumed that $\omega = 314.159$ rad/s (50 Hz), $s\omega = 3.28$ rad/s (1 Hz), and $\omega_r = 37.7$ rad/s (6 Hz). A negative frequency indicates negative phase sequence.

The above analysis is based on a linearized model of the machine. Therefore, the principle of superposition can be used to deal with a general situation with multiple speed ripple components at different frequencies. This is described in the Appendix.

IV. HARMONIC CALCULATION METHOD

Although time-domain simulation can be performed, an analytical method for calculating the harmonics will provide more insight into the mechanism giving rise to the electromechanical interaction. It is also more convenient due to the fact that the harmonic components on the stator and rotor sides will drift on the spectrum during variable speed operation. Based on the above analysis, this section describes a frequency domain method that interrelates the stator and rotor side harmonics, air-gap torque, and speed ripple.

Given current components on the stator and rotor sides, $I_1 \sin(\omega_1 t + \varphi_1)$ and $I_2 \sin(\omega_2 t + \varphi_2)$, the corresponding component in the torque can be calculated as [11]

$$\Delta T_e = -\frac{3PM}{2} I_1 I_2 \sin\left[(\omega_0 - \omega_1 + \omega_2)t - \varphi_1 + \varphi_2\right] \quad (18)$$

In calculating the torque harmonics, it is first assumed that the rotor speed is constant. The above can be modified by substituting $\omega_0 t$ with a Fourier series and applying a Taylor series expansion to the resultant expression. However, this is usually unnecessary as the added harmonic torque components are small. Furthermore, it is usually the torque component due to the interaction between a harmonic current on one side with the fundamental magnetizing current that is of major concern.

The speed ripple corresponding to a harmonic torque component, say $T_h \sin(\omega_h t + \varphi_h)$, can be derived according to the rotor dynamic equation and the result is

$$\omega_{r\_h} = \frac{T_h}{\sqrt{(J\omega_h)^2 + D^2}} \sin\left(\omega_h t + \varphi_h - \tan^{-1}\frac{J\omega_h}{D}\right) \quad (19)$$

where J is the rotor moment of inertia and D the damping ratio. The torque produced by the prime mover would also change with the speed variation. When the torque-speed relationship of the prime mover is linearized, such an effect can be represented collectively in D. Equation (19) can be expanded to include the shaft torsional dynamics, should it be necessary [14].

Using the above, a procedure to calculate the harmonics including the electromechanical interaction in the system can be outlined as follows.

1) Assuming that there is no speed ripple, calculate the fundamental and harmonics in the stator and rotor current. The supply conditions on the two sides of the machine are given. So is the input power/torque of the prime mover. The calculation can be performed using either the steady-state machine equations or the equivalent circuit [7].
2) Calculate the pulsating torque and corresponding speed ripple.
3) For each ripple component in the speed signal, calculate the increment of the impedance matrix according to

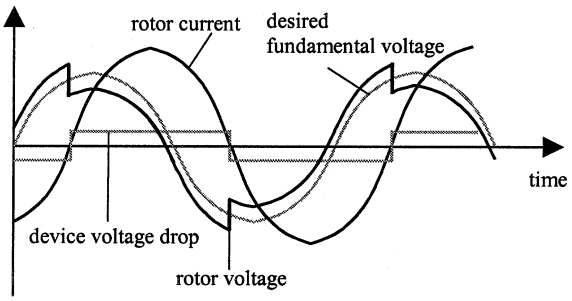

Fig. 3. Generation of low-frequency harmonics in rotor voltage.

(11)–(15). The "d/dt" operator is symbolically retained in the calculation.

4) With the supply voltage on the stator and rotor sides maintained constant, the increment of the current can be determined. It (Δi) can be derived from (17) with $\Delta u = 0$. That is, $\Delta i = -(Z + \Delta Z)^{-1}\Delta Z i \approx -Z^{-1}\Delta Z i$. This is equivalent to a modulation relationship $Z\Delta i \approx -\Delta Z i$. The effect of the original Δu was accounted earlier in step (1). In practice, the calculation for Δi is performed in the frequency domain. For a given speed ripple, frequencies of the elements in ΔZ and the corresponding Δi are also known. Therefore, under the symmetrical condition, the amplitude and phase angle of the incremental current can be directly calculated based on the modulation relationship without the need to compute the inverse of the impedance matrix which may include the system network impedance. In the frequency domain, the "d/dt" operator (p) in ΔZ is translated as "$j\omega$" when it is applied to the fundamental stator current. The derivative operator in the impedance matrix Z is similarly considered.
5) Modify the currents; the results are usually close to the accurate solution. If they need to be more accurate, the procedure can be iterated. Experience shows that one or two iterations are often sufficient.

V. Experimental Validation

The configuration of the laboratory test system is similar to that shown in Fig. 1. The prime mover is a cage induction motor powered by a voltage source of constant amplitude and frequency. The rotor windings of the doubly-fed induction generator are supplied from a PWM inverter. Both machines are of four-pole design and the inverter whose output determines the speed and reactive power operates in the constant volt/Hertz mode. The system is rated at 250 VA and the machine parameters are detailed in the Appendix. Due to the low power rating, the inertia is relatively large; some practical systems would experience more speed ripple than what is to be reported in this paper.

Fig. 3 shows how the rotor PWM inverter, which has a high switching frequency of 1 kHz, can also produce low-frequency harmonics in its output voltage. A train of pulses of different widths synthesizes the desired fundamental voltage. With currents being delivered into the wound rotor windings from the inverter, voltage distortion is introduced due to the voltage drop of the switching devices within the inverter. Fig. 3 shows that the voltage drop is associated with the fundamental current rather than the switching frequency. At a high rotor speed or low slip, the fundamental voltage in the rotor circuit is generally low in amplitude and the rotor windings present a low impedance to the inverter [7]. The low-order harmonics associated with the device voltage drop will cause both a large harmonic current and pulsating torque. It is possible to compensate the effect of the device voltage drop by modifying the switching strategy, but this has not yet been achieved in most commercial inverters without current feedback and complicated calibration tests.

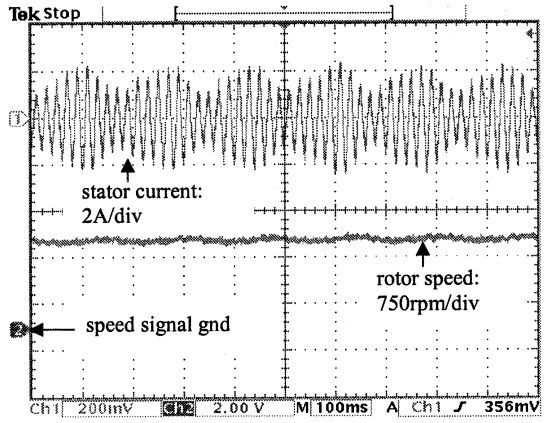

Fig. 4. Measured stator current and rotor speed.

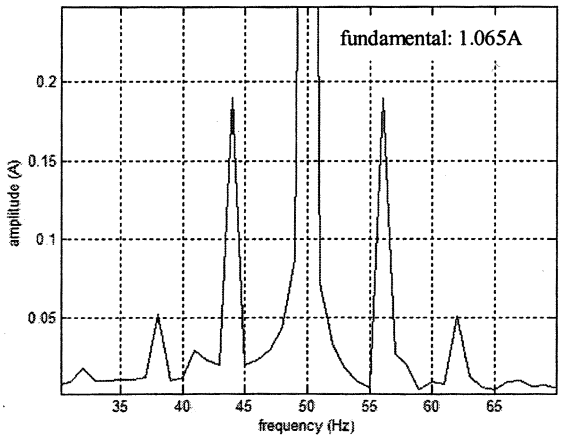

Fig. 5. Spectrum of stator current.

With the inverter fundamental frequency set to 1 Hz and the doubly-fed induction generator running with an average power of 200 W, the speed and stator current of the generator are shown in Fig. 4. Both signals contain ripple at 6 Hz. This is because the rotor supply voltage contains fifth and seventh harmonics of the fundamental. The beating effect of the stator current, particularly its reactive component, will cause voltage fluctuation. A portion of the current spectrum is shown in Fig. 5. In addition to the fundamental at 50 Hz, two distinctive sidebands are present at 50±6 Hz, respectively. Such sidebands are directly linked to the flicker effect as the current flows through the system impedance [15]. Other sideband components are also observed.

Fig. 6 shows the rotor phase-phase voltage and phase current. The voltage waveform consists of many very narrow pulses in order to obtain the required low fundamental voltage. This was

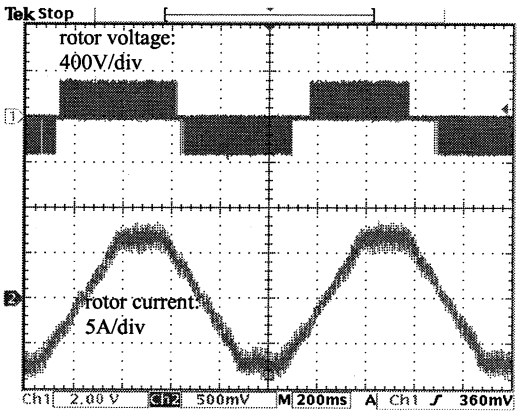

Fig. 6. Measured rotor supply voltage and current.

TABLE II
COMPARISON BETWEEN MEASUREMENT AND CALCULATION

Current (rms)	Measurement	Calculation with speed ripple	Calculation without speed ripple
50 Hz	1.065 A	1.110 A	1.110 A
44 Hz	0.192 A	0.237 A	0.365 A
56 Hz	0.190 A	0.199 A	0.188 A
38 Hz	0.052 A	0.036 A	0.0 A
62 Hz	0.050 A	0.027 A	0.0 A

done because the dc link voltage of the commercial drive used for the laboratory tests was set at 325 V, which was relatively high compared to the required fundamental voltage on the ac side. The dc link voltage could not be further lowered without causing converter tripping on undervoltage protection. Analysis shows that the rms value of the voltage per-phase at 1 Hz, 5 Hz, and 7 Hz are 10.25 V, 1.74 V, and 1.16 V, respectively. Using the measured rotor voltage harmonics and assuming that the mains supply on the stator side is strong, the calculated stator current harmonics (with iteration when considering speed ripple) are compared with the measurement in Table II which shows good agreement when the speed ripple is considered. In the calculation, the torque-speed characteristic of the prime mover is represented using that of the induction motor with a constant supply voltage [13]. Table II also shows that the calculation accuracy is indeed very much dependent on the inclusion of the speed ripple. An error greater than 30% can be caused for the major sidebands if the speed ripple is not included. In this case, ignoring speed ripple gives a pessimistic prediction.

Fig. 7 shows the reconstructed stator current waveform from the calculated harmonic content of the current, with and without including the speed ripple during calculation. The difference is not only the level of the beating effect in the current signal (and, hence, the level of the voltage fluctuation depending on the system impedance) but also how quickly the amplitude of the current increases or decreases in each beating cycle. The signature calculated with the speed ripple included is similar to what was recorded in the experiment (the top trace in Fig. 4).

VI. CASE STUDIES AND DISCUSSION

In order to further illustrate the phenomenon, comparative calculations are performed on a DFIG system rated at 450 kW. The equivalent circuit parameters of the machine are given in the Appendix. The four-pole machine has a typical moment of inertia of 11 $\mathrm{kg.m.}^2$ Depending on the type of the prime mover, the total shaft will certainly have a larger inertia. Regarding the effects of speed ripple, this section will analyze the effects of the moment of inertia and the operating point of the system. With a better understanding of the interaction, possible solutions and design considerations will be discussed.

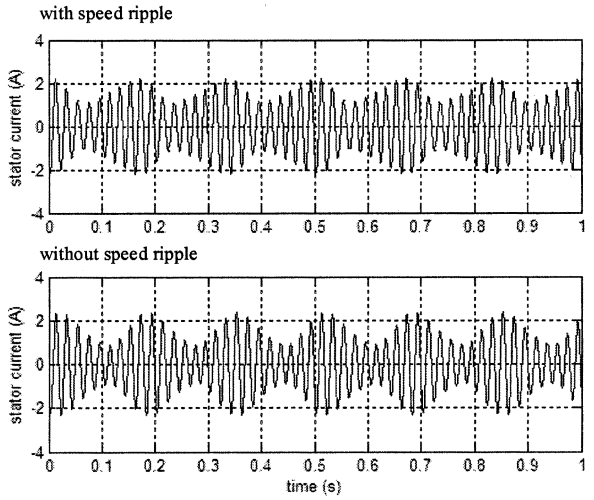

Fig. 7. Stator current reconstructed from calculation.

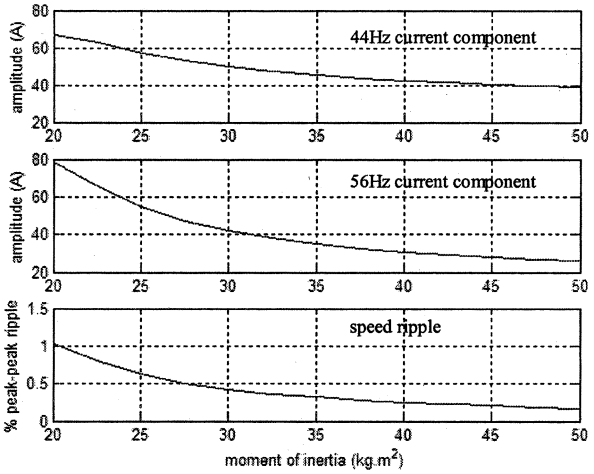

Fig. 8. Sensitivity to moment of inertia.

A. Case 1: Effect of Moment of Inertia

The stator side voltage is 400 V, 50 Hz. The fundamental voltage on the rotor side is at 1 Hz in a rotation direction so that the average rotor speed is 1470 r/min (i.e., below the synchronous speed). The referred amplitude of the per-phase fundamental voltage is 6.73 V(rms). The generator delivers 450-kW real power to the mains system. Without harmonics, the generator would operate at unity power factor. The fifth and seventh harmonics in the rotor supply voltage are 0.254 and 0.174 V, respectively, as referred to the stator side.

Fig. 8 shows the stator current components at 44 and 56 Hz as affected by the shaft inertia. The percentage speed ripple with respect to the average speed is also plotted. For a small pumped storage unit at such a power rating, the total moment of inertia

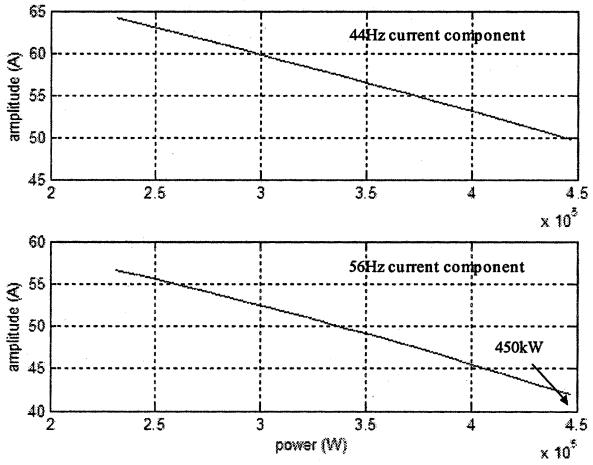

Fig. 9. Effect of operating point.

would be in the range from 20 $\mathrm{kg.m^2}$ to 30 $\mathrm{kg.m^2}$. With wind power generation, the typical value would be around 40 $\mathrm{kg.m^2}$ after the original mass of the wind turbine is referred to the generator side according to the square of the gearbox ratio [16]. In either situation, the rotor speed is subject to some ripple which considerably affects the current signature. Speed ripple can also occur as a result of torsional vibration particularly when the shaft is long, even if the total moment of inertia is large.

B. Case 2: Effect of Operating Point

The moment of inertia is set at 30 $\mathrm{kg.m^2}$. The condition of the stator and rotor supply circuits is the same as in Case 1. Fig. 9 shows the major sidebands of the stator current at 44 and 56 Hz as affected by the real power produced by the generator. A strong dependency is observed. This is because the change of operating condition will affect the interaction between a harmonic current and the fundamental magnetizing current which gives rise to a pulsating torque. As the operating point changes, the damping effect of the generator to the speed ripple will also change. The variation as shown in Fig. 9 will not appear without speed ripple since the harmonic impedance viewed from either side of the machine would otherwise remain constant disregarding the power level.

In the case studies, the assumed harmonics in the rotor supply voltage are justifiable. A practical system can work in different conditions. However, it is shown that the speed ripple can be involved in and will affect the transfer of the low-frequency harmonics from the rotor to the stator sides. In addition to the effect shown earlier in the experiment, the case studies indicate that calculations ignoring the speed ripple may also produce too optimistic results. The original cause for the concern is the low-frequency harmonics on the rotor side. Therefore, to solve this problem, they should be eliminated in the rotor supply voltage. This can be achieved either by modifying the switching strategy of the rotor supply inverter or using an active filter to reduce or eliminate the low-frequency rotor harmonics. It is difficult to deal with the harmonics on the stator side since the current sidebands are close to the fundamental on the spectrum.

VII. Conclusion

This paper analyzes the effects of the low-frequency harmonics on the rotor side of a DFIG. With a PWM inverter supplying the rotor, low-frequency harmonics can be caused by the device voltage drop. It is shown that these harmonics are transferred to the stator side and at the same time will cause speed ripple depending on the inertia and the operating condition of the machine. The speed ripple will modify the amplitudes of the sidebands around the fundamental of the stator current and introduce a series of new components. An analytical method is proposed to evaluate the current spectrum, which can be used to predict the associated voltage fluctuation at the system busbar. Experimental tests are performed to verify the analysis and the calculation method. The tests and numerical case studies show that, for small and medium size systems, it is often necessary to consider the effect of speed ripple. Harmonics could be eliminated at the rotor side by modifying the switching strategy of the inverter or using external compensation.

Appendix A

Derivation and Expansion of $C_{\omega_0+\omega_r}$, $C_{\omega_0-\omega_r}$, $D_{\omega_0+\omega_r}$, and $D_{\omega_0-\omega_r}$

With an incremental rotor electrical angle, the inductance matrix L can be linearized using a first-order Taylor expansion

$$L = \begin{bmatrix} L_s & M_{sr} \\ M_{rs} & L_r \end{bmatrix} = L_0 + \begin{bmatrix} 0 & \Delta M_{sr} \\ \Delta M_{rs} & 0 \end{bmatrix} \tag{20}$$

where L_0 is the original inductance matrix without the angle disturbance. The original rotor angle is calculated as $\theta = \omega_0 t$. It is noted that L_sc consists of the self and mutual inductances of the stator windings. Similarly, L_rc consists of the self and mutual inductances of the rotor windings. All elements in L_s and L_r are constant for the round rotor machine. Therefore, their increments are zero. The mutual inductances between stator and rotor windings are dependent on the rotor angle as shown in (4). Their increments ΔM_{sr} and ΔM_{rs} are expanded below

$$\begin{aligned} \Delta M_{sr} = \Delta M_{rs}^T = & -\frac{2M}{3} \\ & \times \begin{bmatrix} \sin(\omega_0 t) & \sin\left(\omega_0 t + \frac{2\pi}{3}\right) & \sin\left(\omega_0 t - \frac{2\pi}{3}\right) \\ \sin\left(\omega_0 t - \frac{2\pi}{3}\right) & \sin(\omega_0 t) & \sin\left(\omega_0 t + \frac{2\pi}{3}\right) \\ \sin\left(\omega_0 t + \frac{2\pi}{3}\right) & \sin\left(\omega_0 t - \frac{2\pi}{3}\right) & \sin(\omega_0 t) \end{bmatrix} \\ & \times \frac{A_r}{\omega_r} \cos(\omega_r t + \alpha_0). \end{aligned} \tag{21}$$

The sine functions in (21) are due to the derivatives of the stator-rotor mutual inductances (4) with respect to the rotor electrical angle $\theta(= \omega_0 t)$, while $A_r/\omega_r \cos(\omega_r t + \alpha_0)$ is the incremental rotor angle given by (8). Each element in (21) is derived by applying the following first-order Taylor expansion to the corresponding element in (4)

$$\begin{aligned} \cos(\theta + \Delta\theta) &= \cos\theta + \frac{d(\cos\theta)}{d\theta} \cdot \Delta\theta \\ &= \cos\theta - \sin\theta \cdot \Delta\theta. \end{aligned} \tag{22}$$

When components at different frequencies exist in the speed ripple, the incremental rotor angle can be expanded to include

multiple terms and the analysis can be carried out in a similar way based on the superposition principle. Each element in the final resultant 3×3 matrix of (21) is a product of sine and cosine functions, which can be expanded using a trigonometric identity. For instance, the first element (row 1, column 1) is

$$-\frac{2MA_r}{3\omega_r}\sin(\omega_0 t)\cos(\omega_r t+\alpha_0) = -\frac{MA_r}{3\omega_r} \times \sin\left[(\omega_0+\omega_r)t+\alpha_0\right] - \frac{MA_r}{3\omega_r}\sin\left[(\omega_0-\omega_r)t-\alpha_0\right]. \quad (23)$$

Differentiating the right-hand side with respect to time gives the following:

$$-\frac{MA_r}{3\omega_r}(\omega_0+\omega_r)\cos\left[(\omega_0+\omega_r)t+\alpha_0\right] - \frac{MA_r}{3\omega_r}(\omega_0-\omega_r)\cos\left[(\omega_0-\omega_r)t-\alpha_0\right]. \quad (24)$$

Since the impedance matrix is defined as $Z = R + pL + Lp$, the increment due to a speed ripple includes terms which are proportional to the incremental inductance or its derivative. These correspond to (12)–(15). Based on the above analysis, the submatrices in these equations. $C_{\omega_0+\omega_r}$, $C_{\omega_0-\omega_r}$, $D_{\omega_0+\omega_r}$, and $D_{\omega_0-\omega_r}$ should be expanded as shown in the equation at the bottom of the page.

APPENDIX B

TEST MACHINE PARAMETERS

Ratings: 250 VA, 230 V, 50 Hz;
Stator resistance: 6.65 Ω;
Rotor resistance: 5.07 Ω;
Magnetizing inductance: 290 mH;
Moment of inertia: 0.0035 $\mathrm{kg.m^2}$;
Stator leakage inductance: 20 mH;
Rotor leakage inductance: 20 mH.

APPENDIX C

450-kW MACHINE PARAMETERS

Ratings: 450 kW, 0.9 power factor, 400 V, 50 Hz;
Stator resistance: 1.18 $\mathrm{m\Omega}$;
Rotor resistance: 2.8 $\mathrm{m\Omega}$;
Magnetizing inductance: 2.93 mH;
Moment of inertia: 11.0 $\mathrm{kg.m^2}$.

REFERENCES

[1] H. Akagi, "The state-of-the-art of power electronics in Japan," *IEEE Trans. Power Electron.*, vol. 13, pp. 345–356, Mar. 1998.
[2] S. Heier, *Grid Integration of Wind Energy Conversion Systems*. New York: Wiley, 1998, pp. 105–118.
[3] Y. Hu, M. Cirstea, M. McCormick, P. Urwin, and L. Haydock, "Modeling and simulation of a variable speed stand-alone generator system," in *Proc. Inst. Elect. Eng. Int. Conf. Power Electron. Variable Speed Drives*, London, U.K., 2000, pp. 372–377.
[4] B. R. Pelly, *Thyristor Phase-Controlled Converters and Cycloconverters*. New York: Wiley-Interscience, 1971, pp. 278–327.
[5] K. S. Smith and L. Ran, "Input current harmonic analysis of pseudo 12-pulse 3-phase to 6-phase cycloconverters," *IEEE Trans. Power Electron.*, vol. 11, pp. 629–640, July 1996.
[6] A. Larsson, "Flicker emission of wind turbines during continuous operation," *IEEE Trans. Energy Conversion*, vol. 17, pp. 114–118, Mar. 2002.
[7] Z. M. Salameh and L. F. Kazda, "Analysis of the double output induction generator using direct three-phase model, part II—harmonic analysis," *IEEE Trans. Energy Conversion*, vol. 2, pp. 182–188, June 1987.
[8] L. Refoufi and P. Pillay, "Harmonic analysis of slip energy recovery induction motor drives," *IEEE Trans. Energy Conversion*, vol. 9, pp. 665–672, Dec. 1994.
[9] J. Faiz, H. Barati, and E. Akpinar, "Harmonic analysis and performance improvement of slip energy recovery induction motor drives," *IEEE Trans. Power Electron.*, vol. 16, pp. 410–417, May 2001.
[10] R. Yacamini, K. S. Smith, and L. Ran, "Monitoring torsional vibrations of electromechanical systems using stator currents," *J. Vibration Acoust., Trans. Amer. Soc. Mech. Eng.*, vol. 120, pp. 72–79, 1998.
[11] P. C. Krause, O. Wasynczuk, and S. D. Sudhoff, *Analysis of Electric Machinery*. New York: IEEE Press, 1995, pp. 164–206.
[12] Y. Liao, D. Xiang, L. Ran, and G. A. Putrus, "Harmonic transfer in an a.c. excited generator including speed ripple," in *Proc. 28th Annu. Conf. IEEE Ind. Electron. Soc.*, Sevilla, Spain, 2002.
[13] M. G. Say, *Alternating Current Machines*. White Plains, NY: Longman, 1983, pp. 250–259.
[14] L. Ran, R. Yacamini, and K. S. Smith, "Torsional vibrations in electrical induction motor drives during start-up," *J. Vibr. Acoust., Trans. Amer. Soc. Mech. Eng.*, vol. 118, pp. 242–251, 1996.
[15] P. Ashmole, "Quality of supply—voltage fluctuations, part 2," *Inst. Elect. Eng. Power Eng. J.*, vol. 15, no. 2, pp. 108–114, 2001.

$$C_{\omega_0+\omega_r} = -\begin{bmatrix} \cos\left[(\omega_0+\omega_r)t+\alpha_0\right] & \cos\left[(\omega_0+\omega_r)t+\frac{2\pi}{3}+\alpha_0\right] & \cos\left[(\omega_0+\omega_r)t-\frac{2\pi}{3}+\alpha_0\right] \\ \cos\left[(\omega_0+\omega_r)t-\frac{2\pi}{3}+\alpha_0\right] & \cos\left[(\omega_0+\omega_r)t+\alpha_0\right] & \cos\left[(\omega_0+\omega_r)t+\frac{2\pi}{3}+\alpha_0\right] \\ \cos\left[(\omega_0+\omega_r)t+\frac{2\pi}{3}+\alpha_0\right] & \cos\left[(\omega_0+\omega_r)t-\frac{2\pi}{3}+\alpha_0\right] & \cos\left[(\omega_0+\omega_r)t+\alpha_0\right] \end{bmatrix} \quad (25)$$

$$C_{\omega_0-\omega_r} = -\begin{bmatrix} \cos\left[(\omega_0-\omega_r)t-\alpha_0\right] & \cos\left[(\omega_0-\omega_r)t-\frac{2\pi}{3}-\alpha_0\right] & \cos\left[(\omega_0-\omega_r)t-\frac{2\pi}{3}-\alpha_0\right] \\ \cos\left[(\omega_0-\omega_r)t-\frac{2\pi}{3}-\alpha_0\right] & \cos\left[(\omega_0-\omega_r)t-\alpha_0\right] & \cos\left[(\omega_0-\omega_r)t+\frac{2\pi}{3}-\alpha_0\right] \\ \cos\left[(\omega_0-\omega_r)t+\frac{2\pi}{3}-\alpha_0\right] & \cos\left[(\omega_0-\omega_r)t-\frac{2\pi}{3}-\alpha_0\right] & \cos\left[(\omega_0-\omega_r)t-\alpha_0\right] \end{bmatrix} \quad (26)$$

$$D_{\omega_0+\omega_r} = -\begin{bmatrix} \sin\left[(\omega_0+\omega_r)t+\alpha_0\right] & \sin\left[(\omega_0+\omega_r)t+\frac{2\pi}{3}+\alpha_0\right] & \sin\left[(\omega_0+\omega_r)t-\frac{2\pi}{3}+\alpha_0\right] \\ \sin\left[(\omega_0+\omega_r)t-\frac{2\pi}{3}+\alpha_0\right] & \sin\left[(\omega_0+\omega_r)t+\alpha_0\right] & \sin\left[(\omega_0+\omega_r)t+\frac{2\pi}{3}+\alpha_0\right] \\ \sin\left[(\omega_0+\omega_r)t+\frac{2\pi}{3}+\alpha_0\right] & \sin\left[(\omega_0+\omega_r)t-\frac{2\pi}{3}+\alpha_0\right] & \sin\left[(\omega_0+\omega_r)t+\alpha_0\right] \end{bmatrix} \quad (27)$$

$$D_{\omega_0-\omega_r} = -\begin{bmatrix} \sin\left[(\omega_0-\omega_r)t-\alpha_0\right] & \sin\left[(\omega_0-\omega_r)t-\frac{2\pi}{3}-\alpha_0\right] & \sin\left[(\omega_0-\omega_r)t-\frac{2\pi}{3}-\alpha_0\right] \\ \sin\left[(\omega_0-\omega_r)t-\frac{2\pi}{3}-\alpha_0\right] & \sin\left[(\omega_0-\omega_r)t-\alpha_0\right] & \sin\left[(\omega_0-\omega_r)t+\frac{2\pi}{3}-\alpha_0\right] \\ \sin\left[(\omega_0-\omega_r)t+\frac{2\pi}{3}-\alpha_0\right] & \sin\left[(\omega_0-\omega_r)t-\frac{2\pi}{3}-\alpha_0\right] & \sin\left[(\omega_0-\omega_r)t-\alpha_0\right] \end{bmatrix} \quad (28)$$

[16] A. S. Mercer and E. A. Bossanyi, "The use of variable speed drives for active stall regulation," in *Proc. 18th British Wind Energy Assoc. Conf.*, M. Anderson, Ed., Exeter, U.K., 1996, pp. 353–357.

Yong Liao received the M.Eng. degree in electrical machinery and the Ph.D. degree in power system control from Chongqing University, Chongqing, China, in 1988 and 1997, respectively.

Currently, he is a Professor of Electrical Machinery and Apparatus at Chongqing University. From December 2001 to May 2002, he was a Visiting Professor at Northumbria University, Newcastle upon Tyne, U.K. His research interests include the control of doubly-fed electrical machines as used in renewable energy systems.

Li Ran (M'98) received the Ph.D. degree in power systems from Chongqing University, Chongqing, China, in 1989.

Currently, he is with the School of Engineering at the University of Durham, Durham, U.K., where he is responsible for research in Power Electronics in the New and Renewable Energy Group. Until July 2003, he was a Senior Lecturer in Power Electronics at Northumbria University, Newcastle upon Tyne, U.K. From 1992 and 1999, he was a Research Fellow at Aberdeen University, Aberdeen, U.K., Nottingham University, Nottingham, U.K., and Heriot-Watt University, Edinburgh, U.K., where he was involved in research regarding marine and offshore electrical systems. His research interests include power system harmonics, application of power electronics in power systems, and electromagnetic compatibility of power electronic systems.

Ghanim A. Putrus received the Ph.D. degree from the University of Manchester Institute of Science and Technology, Manchester, U.K.

He joined Northumbria University, Newcastle upon Tyne, U.K., as a Senior Lecturer in Power System Engineering in 1995. Since moving to Northumbria, he has provided consultancy to several companies including Northern Electric Distribution Ltd., Newcastle upon Tyne, U.K., VATECH Reyroll National Grid Company (NGC), Coventry, U.K., and Warner Electric, Tyne and Wear, U.K. His research interests include FACTS, custom power technology, power quality, and embedded generation.

Dr. Putrus was a member of the 1999–2000 IEE Professional Group P7. He is still regularly involved in IEE professional activities such as organizing lectures and refereeing papers.

Kenneth S. Smith (M'99) received the Ph.D. degree in electrical engineering from the University of Aberdeen, Aberdeen, U.K., in 1992.

Currently, he is with Mott MacDonald's Power Systems Division in Glasgow, U.K., where he is responsible for power system transient studies. He was an academic staff member at the University of Aberdeen and later Heriot-Watt University, Edinburgh, U.K., for ten years. He held several EPSRC research grants to investigate new methods for marine electrical propulsion and interconnection of offshore oil platforms.